Article

Not peer-reviewed version

Optimizing the Energy Product in Core-Shell Nanoparticle Magnets: Can Hard-and-Fast Rules Be Set?

Ioannis Panagiotopoulos * , Georgia Basina , Garyfalia Nezou , Alexandros Konstadinidis , Vasileios Alexandrakis , Vasileios Tzitzios , George Hadjipanayis

Posted Date: 23 March 2026

doi: 10.20944/preprints202603.1748.v1

Keywords: permanent magnet; energy product; hard-soft magnetic nanocomposites; core-shell magnetic nanoparticles; magnetization reversal

 doi:10.20944/preprints202603.1748.v1

Article

Optimizing the Energy Product in Core-Shell Nanoparticle Magnets: Can Hard-and-Fast Rules Be Set?

Ioannis Panagiotopoulos [1,*], Georgia Basina [2], Garyfalia Nezou [2], Alexandros Konstadinidis [2], Vasileios Alexandrakis [2], Vasileios Tzitzios [2] and George Hadjipanayis [3]

[1] Department of Materials Science and Engineering, University of Ioannina, 45110 Ioannina, Greece

[2] Institute of Nanoscience and Nanotechnology, National Centre for Scientific Research "Demokritos", 15310 Athens, Greece

[3] College of Enginnering, Northeastern University, 360 Huntington Ave, Boston, MA 02115, USA

* Correspondence: ipanagio@uoi.gr

Abstract

The optimization of the energy product in permanent magnets presents a complicated multi-parametric problem that encompasses a large variety of intrinsic and microstructural properties. As both high remanent magnetization and coercivity are required, the main concern in optimizing a given material is often how to deal with the trade-off between these two properties. A promising approach is to combine high anisotropy and high magnetization phases in chemically synthesized magnetically hard-soft nanoparticles. The magnetization reversal in such systems has been studied by micromagnetics, but most of the solutions are given for a magnetically hard shell surrounding a magnetically soft core, though synthetically the opposite may be more convenient. Here we review and summarize the basic general design rules for such systems and we present specific calculations for the FePt/CoFe system. Though in larger particles complex reversal modes appear that are scientifically interesting and may even include topological configurations, these are not relevant to the problem of achieving high energy products. The optimal size and phase content are within the simple homogeneous exchange-spring regime and must be determined under the contradictory requirements of achieving homogeneous reversal and avoiding thermal fluctuations.

Keywords: permanent magnet; energy product; hard-soft magnetic nanocomposites; core-shell magnetic nanoparticles; magnetization reversal

1. Introduction

The figure-of-merit of a permanent magnet is its energy product which represents the energy stored in the magnetostatic field it produces per unit volume [1]. A high energy product magnet can produce strong magnetostatic fields in a large region without itself being bulky.

Unfortunately, the optimization of the energy product in permanent magnets presents a complicated multi-parametric problem that encompasses a large variety of intrinsic and microstructural properties.

As both high remanent magnetization and coercivity are required, the main concern in optimizing a given material is often how to deal with the trade-off between these two properties.

A rule of thumb can be set, by assuming a square M vs H hysteresis curve with remanence M_R and coercivity H_C leading to the conclusion that the maximum energy product is

$$(BH)_{max} = \mu_0(M_R/2)^2 \text{ for } H_C \geq M_R/2,$$
$$(BH)_{max} = \mu_0(M_R - H_c)H_c \text{ for } H_C < M_R/2 \quad (1)$$

the latter is referred to as the "coercivity limited case". Such a perfect square M vs H hysteresis can be achieved in highly-oriented magnets and sets the upper limit for all other cases. A nice

 doi:10.20944/preprints202603.1748.v1

example of the use of (Equation 1) is the optimization of the volume fraction *f* of magnetic particles in purely shape anisotropy magnets consisting of elongated magnetic particles bonded in a non-magnetic matrix. In this case $M_R = fM_s$ and assuming homogeneous "Stoner-Wohlfarth" switching $H_C = 0.5(1-f)M_s$ leading to an optimal $(BH)_{max} = \mu_0 M_S^2/12$ for *f*=2/3 [2]. Higher values can be obtained if uniaxial magneto-crystalline anisotropy also exists along the same axis as in chemically synthesized cobalt nanorods [3]. Of course, beyond this simple rule of thumb any deviation from squareness in the demagnetization quadrant has a significant effect on the $(BH)_{max}$. Figure 1 compares three characteristic cases: (a) a perfect square loop material with $H_C \geq M_R/2$, (b) a non-square loop with the same coercivity and (c) a square loop but with coercivity limited material.

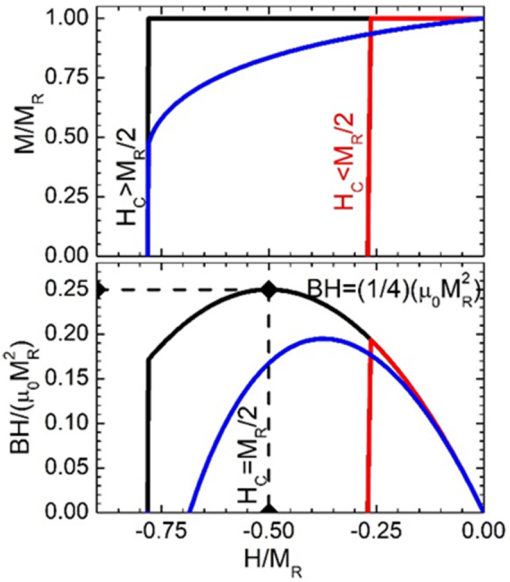

Figure 1. Example demagnetization quadrant *M vs H* curves (upper panel) and corresponding *BH vs H* curves (bottom panel). For generality the quantities *M* and *H* are normalized in M_R and the energy product in $(BH)_{max} = \mu_0 M_R^2$ units. The black curves denote a perfect square loop material with $H_C > M_R/2$ which reaches the optimal value $(BH)_{max} = 0.25\mu_0 M_R^2$. The blue curves give an example of a material with the same coercivity which gives lower $(BH)_{max} = 0.20\mu_0 M_R^2$ due to its non-square loop shape. The red curves give an example of a material with square loop in which $(BH)_{max}$ is clearly coercivity limited $H_C < M_R/2$.

The advent of rare-earth intermetallics marked a revolution in permanent magnet materials thanks to the unique electronic structure of rare-earth elements. These elements exhibit an exceptionally high magnetocrystalline single-ion anisotropy due to the strong spin–orbit coupling of their localized 4f electrons [1]. This intrinsic anisotropy provided a robust mechanism to lock the magnetic moments along preferred crystallographic directions, dramatically enhancing coercivity. However, the saturation magnetization of rare-earth intermetallics themselves is relatively modest. For instance, $Nd_2Fe_{14}B$ having saturation magnetization of $\mu_0 M_s = 1.61\ T$ can give up to $(BH)_{max} = 516\ \mathrm{kJ/m^3}$ according to (Equation 1). Iron with $\mu_0 M_s = 2.15\ T$ would give $(BH)_{max} = 920\ \mathrm{kJ/m^3}$ if it could be made with sufficiently high coercivity, but this is not feasible because of its low magnetocrystalline anisotropy. Then, an obvious idea is to combine high magnetization phases with high anisotropy phases (to provide coercivity) in appropriate nanostructures that result in smooth "one-phase-like" hysteresis with tailor-made M_s and H_C [4–9].

These nanocomposites have been achieved in melt-spun [10–12], mechanically alloyed [13–15] and multilayered thin film structures [8]. One may argue that even $Nd_2Fe_{14}B$ is a naturally made multilayered structure consisting of alternating crystallographic planes of Nd and Fe in atomic ratios that optimize anisotropy and magnetization. However, the outlook of discovering optimized ternary or more complex phases properties seems poor, although recently a high entropy alloy approach is

 doi:10.20944/preprints202603.1748.v1

being explored based on creating artificial multielements as building blocks to discover and stabilize novel microstructures [16].

Another possible geometry towards hard-soft nanocomposites with well controlled nanostructures is based on the chemical synthesis of hard-soft nanoparticles [17] preferentially with core-shell morphology [18–23]. One can note that there is less experimental work on fully metallic systems [22,23]. As a general guideline, since the optimal composition boils down to finding the maximum soft phase content which increases the magnetization without a detrimental loss of coercivity it is expected that the optimized compositions would be in the vicinity of those compositions leading to "coercivity limited" BH_{max}.

2. Can Simple Design Rules Be Set up for the Optimization of Nanocomposite Permanent Magnets?

As regards remanence, a simple rule-of-thumb can be used as its value depends on the easy axis distribution and the magnetic material packing fraction f and scales as:

$$M_R = f\langle cos\theta\rangle M_S \quad (2)$$

where θ is the angle between the anisotropy axis and the field. This equation is valid for materials with uniaxial anisotropy which are the typical materials of choice for permanent magnet applications. In an "isotropic material" with completely random distribution of easy axes $\langle cos\theta\rangle = 1/2$. Thus, the attainable energy product in isotropic magnets is only ¼ of that of highly oriented materials, but the required coercivity is also lower according to Equation 1. We must note here that in nanomaterials with strong intergrain coupling "remanence enhancement" above the values of Equation 2 may be observed. This enhancement has been observed both in single-phase and nanocomposite materials consisting of a fine mixture of soft and hard phases [24]. In a typical permanent magnet manufacturing process both f and $\langle cos\theta\rangle$ are optimized: to obtain a compact with maximum remanent magnetization, the metallic powders are aligned and pressed under field such that the easy axes of magnetization of the powders are parallel. Then, sintering is carried out either in vacuum, inert gas atmospheres or reducing atmospheres to achieve the highest density possible without significant loss of coercivity [25].

For magnets made by compacting chemically synthesized magnetic particles let us note that the theoretical packing fraction limit for cylindrical particles is close to f=0.9 [3] while for spheres f=0.74 [26]. Thus, in principle, according to (Equation 2) cylindrical particles can achieve 33% higher $(BH)_{max}$ compared to spherical ones.

The situation is much more complex when it comes to predicting the coercivity and the loop shape in general. Any deviation from squareness, increased permeability or discontinuous jumps at the demagnetization quadrant is detrimental to the energy product. These characteristics are very sensitively dependent on the exact microstructure characteristics making the establishment of hard-and-fast materials design rules difficult.

In the case of hard-soft nanocomposites again the magnetization is simply equal to the volume average of the magnetizations of the two phases, but this is not necessarily true for other quantities and especially the coercivity [27]. The typical magnetization reversal proceeds by nucleation in the soft phase and propagation to the hard phase. If, after the nucleation propagation does not occur, the coercive field is defined by the propagation. The critical fields depend, apart from the parameters of each phase, on the microstructure and interfacial coupling between the two phases.

The mechanisms of nucleation and propagation are more easily separated and modelled in multilayer [28] or cylindrical structures [29] that can be reduced to 1D models [30]. In some cases, even macro-spin models may give a good approximation [31].

It is often considered that if the two phases are rigidly coupled, and the dimensions below a critical thickness, the composite system is characterized by the averaged magnetic properties of the two layers, yielding a nucleation field [8,32]:

$$H_N = \frac{2(p_H K_H + p_S K_S)}{p_H M_H + p_S M_S} \quad (3)$$

 doi:10.20944/preprints202603.1748.v1

where p_H, p_S are the volume fractions of the hard and soft phase respectively. However, the validity of this simple composite material rule is obviously limited to very fine dispersions of the two phases. In general, the phases must be suitably dispersed and mutually exchange-coupled, to avoid independent switching of the two phases giving rise to what is termed as "stepped", "shouldered" or "wasp-waist-like" hysteresis and maintain sufficiently high coercivity. The nucleation scales with the dimension L of the soft phase as $1/L^2$ while propagation depends on the difference of domain wall energies between the two phases [33]. The main criterion could be set by the distance to the nearest hard region [27] keeping in mind that the critical dimensions are in the nm range following the magnitude of typical magnetic characteristic lengths as exchange lengths (L_{ex}) and domain wall widths.

In nanoparticles the reversal mechanism is more complex. Even in single-domain and single-phase materials, above a critical diameter, an inhomogeneous reversal ("curling" mode) becomes favorable because it follows a "pole-avoidance" path that reduces the magnetostatic contribution by the formation of a vortex-like intermediate state [34,35]. While the homogeneous "Stoner-Wohlfarth" reversal for spherical particles predicts a coercive field of $H_C^{SW} = 2K/\mu_0 M_s$ curling occurs at a field

$$H_C^{Curl} = \frac{2K}{\mu_0 M_s} - \frac{1}{3} M_S + \frac{8.666\, A_{ex}}{\mu_0 M_S R^2} \quad (4)$$

where Aex is the exchange stiffness. Curling which becomes favorable for radii

$$R > R_c = 3.6 L_{ex}, L_{ex} = \sqrt{2A_{ex}/(\mu_o M_S^2)} \quad (5)$$

When it comes to spherical soft/hard particles two separate cases can be distinguished:

When a soft-magnetic core is surrounded by an infinitely hard-magnetic phase nucleation is realized by a mode called "bulging" which is considered to have radial angular symmetry of the coherent mode [36]. If the demagnetizing fields are accurately taken into account, the bulging mode ceases to be an eigenmode for nucleation. At small core sizes, the nucleation of magnetic reversal proceeds via a modified bulging mode, where the transverse component of the magnetization is only semi-coherent in direction and the nucleation field contains a contribution from self-demagnetization [37]. In this case the coercivity has similar dependence with (Equation 3)

$$H_C^{mbulg} = \frac{2K}{\mu_0 M_s} - \frac{1}{3}(M_S - M_H) + \frac{19.74 A_{ex}}{\mu_0 M_S R^2} + 0.975 M_s \quad (6)$$

For large core sizes, the modified curling mode, where the magnetization configuration is vortex-like, is favored at $R > R_c = 3.25 L_{ex}$. It has a vanishing demagnetizing field because of the flux closure.

$$H_C^{mcurl} = \frac{2K}{\mu_0 M_s} - \frac{1}{3}(M_S - M_H) + \frac{40.382 A_{ex}}{\mu_0 M_S R^2} \quad (7)$$

Analytical expressions for the case of a hard magnetic core surrounded by a soft magnetic shell are scarce and mostly given for cylindrical structures [37]. The dipolar field generated from the core is expected to impact the magnetization reversal [38] since in the equatorial region it is directly opposite to the initial magnetization direction (Figure 3). Its inhomogeneous nature is expected to favor the formation inhomogeneous modes of reversal as curling and flower modes in the surrounding shells, although these effects would manifest only for sufficiently thick shells.

 doi:10.20944/preprints202603.1748.v1

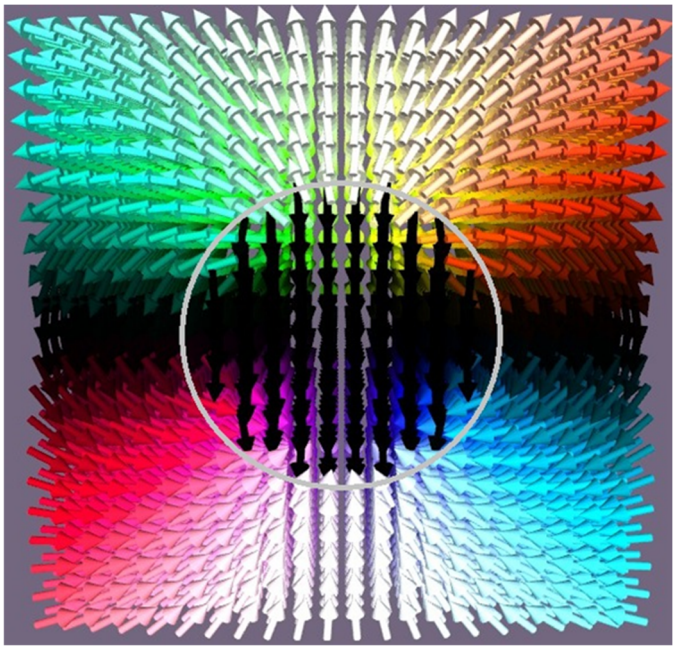

Figure 2. Typical stray field created around a hard phase sphere homogeneously magnetized upwards.

3. The FePt/CoFe Core/Shell System

Here we focus on FePt/CoFe as an example system using micromagnetic simulations performed by the mumax3 finite difference micromagnetic simulation program [39–41]. Monodisperse FePt nanoparticles can be synthesised by chemical liquid phase high-temperature reduction approaches, in high boiling point organic solvents with the presence of a variety of capping agents and have been extensively studied since the seminal work of Sun [42]. The preparation can be followed by annealing to induce $L1_0$ chemical ordering and therefore high anisotropy. Using coercivity vs pulse width data a high uniaxial anisotropy of 5.9×10^6 J/m^3 was estimated for 4 nm particles. The use of bismuth additives in the reaction permits a direct one-step liquid phase chemical approach [43–46]

The Co-Fe alloys, typically used as soft magnetic materials, give a record magnetization of 1.95 MA/m, for the composition $Co_{35}Fe_{65}$. High saturation values are in principle (according to the Slater-Pauling curve) obtained up to the equiatomic composition though the numbers reported in the literature vary depending on the partial chemical ordering, exact composition, impurities and existence of dead or oxide layers in films and particles. Liu and coworkers give for the near equiatomic ($Fe_{53}Co_{47}$) films Ms=1.35 MA/m [47]. For $Fe_{52}Co_{48}$ 1.9 MA/m is used [48] and for equiatomic FeCo nanowires 1.71 MA/m [49]. Interestingly FeCo nanoalloys can be chemically synthesized in liquid phase reactions with the abil-ity to control their sizes in the nanosize regime. [50] Interestingly, CoFe by itself could make high-performance magnet since it is predicted that by chemical ordering to a bct phase with optimized parameter of c/a = 1.20−1.25, can achieve a high value of Ku ≈ 10 MJ/m^3 which is higher than that of FePt [51]. However, this has been achieved in thin films mainly by taking advantage of epitaxial strain in carefully designed multilayer systems [52–54]. An equivalent approach in nanoparticle systems is to grow FeCo shells on AuCu cores thermally treated to induce transformation to the tetragonal $L1_0$ phase [55]. The AuCu was chosen due to lattice matching. Above a critical shell thickness (3.17 nm), the FeCo shell returns to the bcc structure via strain relaxation. This is scientifically interesting but as a permanent magnet its (BH_{max}) is limited by the low volume fraction of the magnetic phase leading to low remanence. For instance, assuming close packed spherical particles with 3.5 nm magnetic shell on 10 nm AuCu core the volume fraction will be 0.48. For a saturation magnetization of 1.8 MA/m the maximum achievable energy product is 240 kJ/m^3. In comparison using single phase FePt nanoparticles with magnetization just 1.1MA/m the maximum achievable energy product is 210 kJ/m^3. Ideally one should seek to achieve the same kind of templated growth on a magnetic $L1_0$ phase with the appropriate lattice constant.

 doi:10.20944/preprints202603.1748.v1

For the hard phase the following parameters of the equiatomic chemically ordered FePt (with the tetragonal $L1_0$ structure) are used: Saturation magnetization M_S=1.1 MA/m, uniaxial anisotropy K_{mc}= 4.9 MJ/m^3 and exchange stiffness A_{ex}=10 pJ/m [42,56–58]. For the CoFe different values are given depending on the exact composition and chemical ordering. In this study the following were assumed: M_S=1.8 MA/m, K_{mc}= 10 kJ/m^3, A_{ex}=25 pJ/m [48,59,60]. A small misalignment of 1.0 deg with the applied field was introduced to avoid numerical errors that could arise in the case where the axes of the magnetocrystalline, and applied field coincide.

In Figure 3, the various types of pathways of the magnetization reversal are summarized as a function of the magnetically hard core diameter and total particle diameter. We can distinguish three qualitatively different regimes. For small diameters the reversal proceeds by a homogeneous canting of the soft shell which increases with the applied reversed field until this state is destabilized and leads to an abrupt reversal to the homogenous reversed state ($m = M/M_s = -1$). Above a critical thickness D_1 which depends weakly on the hard phase diameter (ranging between 28 nm and 30 nm) the reversal proceeds by a curling mode. The axis of the vortex tilts slightly with the applied reversed field until the state is destabilized and an abrupt reversal to the homogenous reversed state (m=-1) occurs. Above a second critical thickness D_2 which depends strongly on the hard phase diameter the reversal proceeds by a curling mode in which a reversed vortex state is also formed. The axis of the vortex tilts slightly with the applied reversed field until the vortex is reversed. This reversed vortex evolves gradually by spin-canting towards the z-axis to the final homogenous reversed state (m=-1).

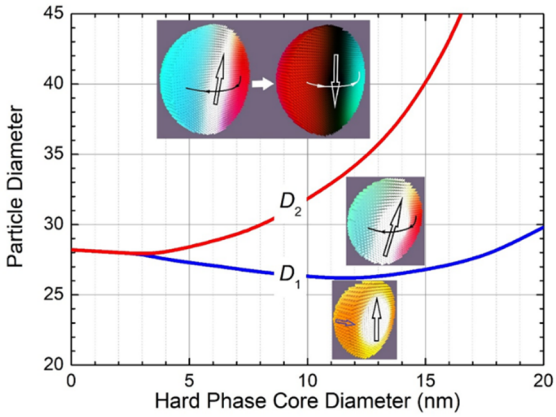

Figure 3. Diagram of different modes of reversal occurring as a function of the hard phase core and total diameter of core-shell nanoparticles. Below a critical thickness D_1 the reversal proceeds by a homogeneous canting of the soft shell. Above D_1 the reversal proceeds by a curling mode which also includes the formation of a reversed vortex above D_2. The insets show characteristic spin configurations for each region. Used color code: White spin up, black spin down, red spin outwards, blue spin inwards, yellow spin to the right.

Typical corresponding demagnetization curves for four cases (points on Figure 3) are shown in Figure 4. A hard phase core of 10 nm with different diameters have been selected. A rapid loss of coercivity and squareness is observed with particle size even for the homogeneous canting regime. The existence of non-homogeneous modes of reversal leads to severe reduction of the magnetization in the demagnetization quadrant of the hysteresis loop which is deleterious to the $(BH)_{max}$. Although these modes are scientifically interesting (and even lead to the existence of topologically non-trivial configurations [61]) for permanent magnet applications the particle size should be restricted below 26 nm.

 doi:10.20944/preprints202603.1748.v1

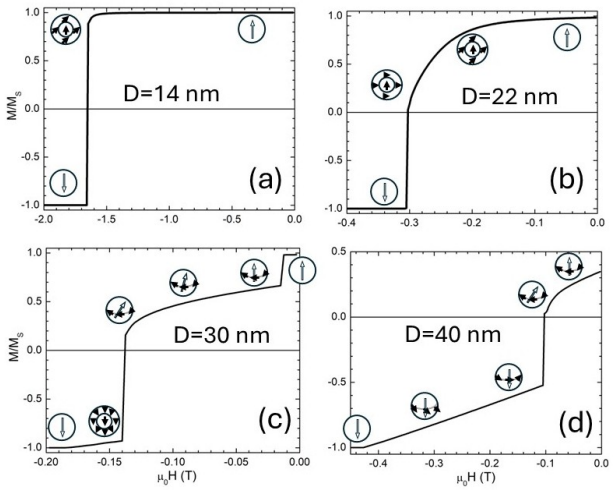

Figure 4. Typical demagnetization curves corresponding to three cases of Figure 3. In all cases the magnetic hard phase diameter is 10 nm. (a) Particle diameter 14nm: the reversal starts with a small homogeneous canting of the soft shell which destabilizes the particle and leads to an abrupt reversal. (b) Particle diameter 22nm: the reversal proceeds by a gradual homogeneous canting of the soft shell and loss of squareness which increases with the applied reversed field until this state is destabilized followed by an abrupt full reversal. (c) Particle diameter 30nm: the reversal proceeds by a curling mode which includes the formation of a vortex is destabilized and followed an abrupt reversal to a reversed state. (d) Particle diameter 40nm: the reversal proceeds by the formation of a vortex which is reversed and gradually tilts towards the completely reversed state.

These simulations further show that Equation 3 holds for very small diameters. Using Equation 3 one can calculate, for the given FePt and CoFe phase parameters, a maximum $(BH_{max})=505$ kJ/m^3 achieved for hard phase content $p_H=0.12$ (the compositions with $p_H<0.126$ being coercivity limited). In other words, the hard phase core could be almost half (equal to 0.4936) of the total diameter.

Comparison of the coercivities derived by our simulations to the predictions of Equation 3 are presented on Figure 5. Only the D=6 nm case is close to the predictions of Equation 3.

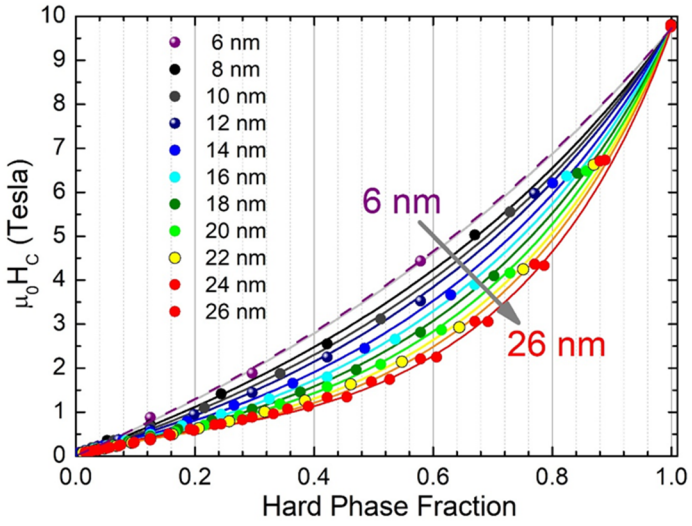

Figure 5. Coercivity vs Hard Phase fraction for core/shell nanoparticles of different diameters (indicated in nm). The simple composite material rule implied by eq.3 (dashed line) can only describe the 6 nm particles. For the higher diameters strong deviations are observed that can be phenomenologically described by Equation 8 (continuous lines).

 doi:10.20944/preprints202603.1748.v1

For the rest of the cases the data can be phenomenologically fitted by assuming volume fraction corrected by an additional non-linear term which increases with diameter. We have used the form for the effective volume fraction:

$$p_H^{eff} = p_H + a \cdot p_H^n \ln(p_H) \quad (8)$$

Note that the data (as well as Equation 8) imply that for either $p_H = 0$ or 1 the Stoner-Wohlfarth prediction holds (as $p_H^{eff} = p_H$). Thus, it is the two-phase nature of the particles that enhances the deviations from the simple Stoner-Wohlfarth prediction which is reasonable due to the spherical geometry with inhomogeneous radial profile. For the data of Figure 5 the non-linear part scales with the diameter as $a = (D - 16.1\text{nm})/15.3\text{nm}$ while the exponent n varies between n=1.4 and n=1.8.

On the other hand, the paramagnetic size for the hard phase can be calculated to D_p=3.2 nm. Therefore, sizes must be well above 3.2 nm to avoid a reduction of the coercivity of the order of $(D_p/D)^{3/2}$. In conclusion, zero temperature calculations cannot be safely used for the prediction of coercivity and energy products. Even for 26 nm the expected thermal reduction of coercivity is close to 4% meaning that in this range of diameters the temperature effects cannot be ignored. The optimal size and phase content must be determined under the conflicting requirements of having a particle size small enough to achieve a homogeneous reversal and large enough to avoid thermal fluctuations.

To take into account thermal effects, a reduction of coercivity of the order of $1 - \sqrt{T/T_B}$ (at T=300K) was assumed and the blocking temperature was calculated using the relation $25k_BT_B = V_HK_H + V_SK_S$. This simple textbook formula is derived assuming an Arrhenius law with fixed attempt frequency of 1 GHz [1]. In fact, the results of mumax3 simulations at finite temperature [39] are compatible with a field-dependent attempt frequency as analyzed in [62]. This model equivalently gives a sharply peaked attempt frequency of the order of 1 GHz for applied reversed fields close to the anisotropy field. Let us also note that, thermal fluctuations induce more homogeneous modes of reversal compared to applied field. This principle, which permitted the optimization of exchange spring recording media [63] implies that temperature is not expected to affect the loop squareness unless a broad particle size distribution is present.

Taking all these factors into account (Figure 6), the maximum energy product of 462 kJ/m³ is obtained for a particle of 11.7 nm with a FePt core of 7.1 nm (p_H=0.223)

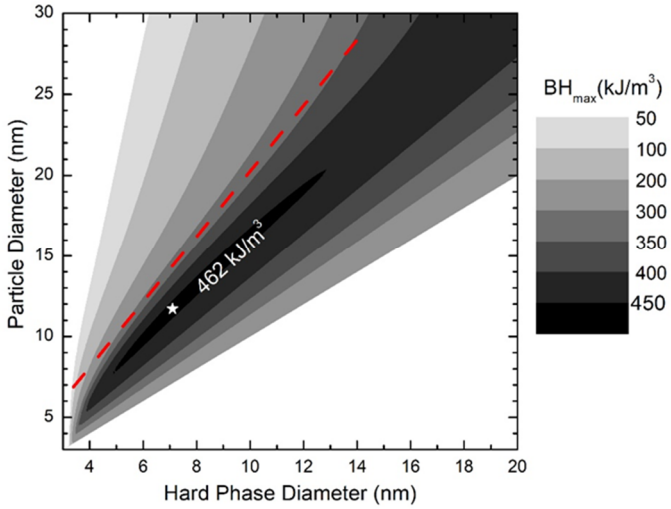

Figure 6. Energy product contour plot as a function of the hard phase diameter core and total particle diameter. The dashed red line shows the locus of the maximum energy product according to Equation 3 and without taking on account the temperature effects. Taking these extra factors into account slightly larger hard phase content is needed.

 doi:10.20944/preprints202603.1748.v1

4. Discussion and Conclusions

The idea to create high performance magnets by fabricating nanocomposites consisting of high magnetization and high anisotropy phases dates back several decades [5] but has attracted the uninterrupted interest of scientific community which has intensified lately due to the recent instabilities in rare earths supply [64]. The rich variety of possible existing systems, and complex reversal mechanisms that they may exhibit, make it seem impossible at first sight to set-up some hard-and-fast design rules. However, keeping in mind that deviation from loop squareness is detrimental to the $(BH)_{max}$ makes obvious that optimized systems should consist of small entities that are characterized by homogeneous reversal modes. More complex modes though are scientifically very interesting and may include topological configurations are not relevant to the problem of achieving high energy products. In short, the optimal size and phase content must be determined under the contradictory requirements of achieving homogeneous reversal and avoiding thermal fluctuations. One should keep in mind that any reduction in magnetic packing fraction, as the use of bonding materials, reduces the energy product by the square of the packing fraction. In this respect spherical nanoparticles are disadvantageous as in principle they can achieve a maximum packing fraction of f=0.74. In contrast, in needle-like particles f=0.9 is achievable. Aligning in a magnetic field is straightforward and in principle can quadruple the energy product so it should be done. Here we have used micromagnetic simulations to analyze the FePt/CoFe hard magnetic core /soft magnetic shell system. However, the same method can be applied to any geometry.

Author Contributions: Conceptualization, I. Panagiotopoulos and V. Tzitzios; methodology, I. Panagiotopoulos.; software, investigation, data curation, G Basina, G Nezou, A Konstadinidis; writing—original draft preparation, I. Panagiotopoulos.; writing—review and editing, V. Tzitzios, V Alexandrakis, G Hadjipanayis, G Basina; supervision V. Tzitzios.; funding acquisition, V. Tzitzios. All authors have read and agreed to the published version of the manuscript.

Funding: This research was funded by Hellenic Foundation for Research and Innovation (H.F.R.I.) under the grand «Nanostructured Non-rare earth sustainable Magnets Acronym: NaNoMag/23714».

Institutional Review Board Statement: Not applicable" for studies not involving humans or animals.

Informed Consent Statement: Not applicable.

Data Availability Statement: All data and mumax3 scripts are available upon request.

Conflicts of Interest: The authors declare no conflicts of interest.

Abbreviations

The following abbreviations are used in this manuscript:

MDPI	Multidisciplinary Digital Publishing Institute
DOAJ	Directory of open access journals
TLA	Three letter acronym
LD	Linear dichroism

References

1. See for instance Coey, J.M.D. Magnetism and Magnetic Materials; Cambridge University Press: Cambridge, UK, 2010; . Cullity, B.D.; Graham, C.D. Introduction to Magnetic Materials, 2nd ed.; Wiley: Hoboken, NJ, USA, 2011.; Krishnan, K.M. Fundamentals and Applications of Magnetic Materials; Oxford University Press: Oxford, UK, 2016.
2. Skomski, R.; Liu, Y.; Shield, J.E.; Hadjipanayis, G.C.; Sellmyer, D.J. Permanent magnetism of dense-packed nanostructures. J. Appl. Phys. 2010, 107, 09A739. https://doi.org/10.1063/1.3337657

 doi:10.20944/preprints202603.1748.v1

3. Panagiotopoulos, I.; Fang, W.; Ott, F.; Boué, F.; Aït-Atmane, K.; Piquemal, J.-Y.; Viau, G. Packing fraction dependence of the coercivity and the energy product in nanowire-based permanent magnets. J. Appl. Phys. 2013, 114, 143903. https://doi.org/10.1063/1.482438
4. Kneller, E.F.; Hawig, R. The exchange-spring magnet: A new material principle for permanent magnets. IEEE Trans. Magn. 1991, 27, 3588–3590. https://doi.org/10.1109/20.102931
5. Skomski, R., & Coey, J. M. D. (1993). Giant energy product in nanostructured two-phase magnets. Physical Review B, 48(21), 15812. 10.1103/physrevb.48.15812
6. Skomski, R. Aligned two-phase magnets: Permanent magnetism of the future? J. Appl. Phys. 1994, 76, 7059–7064. https://doi.org/10.1063/1.358027
7. Schrefl, T.; Fidler, J.; Kronmüller, H. Remanence and coercivity in isotropic nanocrystalline permanent magnets. Phys. Rev. B 1994, 49, 6100–6108. https://doi.org/10.1103/PhysRevB.49.6100
8. Fullerton, E.E.; Jiang, J.S.; Bader, S.D. Hard/soft magnetic heterostructures: Model exchange-spring magnets. J. Magn. Magn. Mater. 1999, 200, 392–404. https://doi.org/10.1016/S0304-8853(99)00376-5
9. Sellmyer, D.J. Strong magnets by self-assembly. Nature 2002, 420, 374–375.
10. Manaf, A.; Buckley, R.A.; Davies, H.A. New nanocrystalline high-remanence Nd–Fe–B alloys by rapid solidification. J. Magn. Magn. Mater. 1993, 128, 302–306. https://doi.org/10.1016/0304-8853(93)90475-H
11. Withanawasam, L.; Hadjipanayis, G.C.; Krause, R.F. Enhanced remanence in isotropic Fe-rich melt-spun Nd–Fe–B ribbons. J. Appl. Phys. 1994, 75, 6646–6648. https://doi.org/10.1063/1.356882
12. Withanawasam, L., Panagiotopoulos, I., & Hadjipanayis, G. C. Melt-spun Pr2Co14B/Co nanocomposite magnets. J. Appl. Phys. 1996, 79, 4837-4839. https://doi.org/10.1063/1.361625
13. Ding, J.; McCormick, P.G.; Street, R. Remanence enhancement in mechanically alloyed isotropic Sm7Fe93 nitride. J. Magn. Magn. Mater. 1993, 124, 1–4. https://doi.org/10.1016/0304-8853(93)90060-F
14. Gabay, A.M.; Hadjipanayis, G.C. Application of mechanochemical synthesis to manufacturing of permanent magnets. JOM 2015, 67, 1329–1335. DOI: 10.1007/s11837-015-1426-4
15. Anuraag, N.S.; Shaw, S.K.; Upadhyay, C.; Prasad, N.K. Mechanochemical synthesis of MnBi/Fe3C@C exchange-coupled hard magnetic nanocomposites. J. Solid State Chem. 2024, 329, 124403. https://doi.org/10.1016/j.jssc.2023.124403
16. Na, S.M.; Lambert, P.K.; Jones, N.J. Hard magnetic properties of FeCoNiAlCuXTiX-based high-entropy alloys. AIP Adv. 2021, 11, 015217. https://doi.org/10.1063/9.0000097
17. Figuerola, A.; et al. One-pot synthesis and characterization of size-controlled bimagnetic FePt–iron oxide heterodimer nanocrystals. J. Am. Chem. Soc. 2008, 130, 1477–1487. https://doi.org/10.1021/ja078034v
18. Zeng, H.; Sun, S.; Li, J.; Wang, Z.L.; Liu, J.P. Tailoring magnetic properties of core/shell nanoparticles. Appl. Phys. Lett. 2004, 85, 792–794. https://doi.org/10.1063/1.1776632
19. Masala, O., Hoffman, D., Sundaram, N., Page, K., Proffen, T., Lawes, G., & Seshadri, R. Preparation of magnetic spinel ferrite core/shell nanoparticles: Soft ferrites on hard ferrites and vice versa. Solid state sciences 2006, 8(9), 1015-1022. https://doi.org/10.1016/j.solidstatesciences.2006.04.014
20. Nandwana, V.; et al. Bimagnetic nanoparticles with enhanced exchange coupling and energy products. J. Appl. Phys. 2009, 105, 013901. https://doi.org/10.1063/1.3054441
21. López-Ortega, A., Estrader, M., Salazar-Alvarez, G., Roca, A. G., & Nogués, J. Applications of exchange-coupled bi-magnetic core/shell nanoparticles. Phys. Rep. 2015, 553, 1–32 https://doi.org/10.1016/j.physrep.2014.09.007 and references therein.
22. Li, D., Wang, H., Ma, Z., Liu, X., Dong, Y., Liu, Z., & Jiang, C. FePt/Co core/shell nanoparticle-based anisotropic nanocomposites. Nanoscale 2018, 10, 4061–4067. https://doi.org/10.1039/C8NR00190A
23. Quan, W., Yao, L., Zheng, Q., Si, P., Bian, B., & Du, J. (2022). High-performance anisotropic nanocomposites with a novel core/shell microstructure. ACS Appl. Mater. Interfaces 2022, 14, 15558–15564. https://doi.org/10.1021/acsami.2c01817
24. Panagiotopoulos, I., Withanawasam, L., & Hadjipanayis, G. C. (1996). Exchange spring behavior in nanocomposite hard magnetic materials. J. Magn. Magn. Mater. 1996, 152, 353–358. https://doi.org/10.1016/0304-8853(95)00467-X

 doi:10.20944/preprints202603.1748.v1

25. Cui, J., Ormerod, J., Parker, D., Ott, R., Palasyuk, A., Mccall, S., Lograsso, T. et al. Manufacturing processes for permanent magnets: Part I—Sintering and casting. JOM 2022, 74, 1279–1295. https://doi.org/10.1007/s11837-022-05156-9
26. Jiang, J. S., & Bader, S. D. Rational design of the exchange-spring permanent magnet. J. Phys. Condens. Matter 2014, 26, 064214. http://dx.doi.org/10.1088/0953-8984/26/6/064214
27. Skomski, R. (Simple Models of Magnetism; Oxford University Press: Oxford, UK, 2008 (§4.7.5)
28. Zhao, G. P., Zhao, M. G., Lim, H. S., Feng, Y. P., & Ong, C. K. From nucleation to coercivity. Appl. Phys. Lett. 2005, 87, 162513. https://doi.org/10.1063/1.2108120
29. Loxley, P. N., & Stamps, R. L. Theory for nucleation at an interface and magnetization reversal. Phys. Rev. B 2006, 73, 024420. https://doi.org/10.1103/PhysRevB.73.024420
30. Amato, M.; Pini, M.G.; Rettori, A. Optimization study of hard/soft magnetic multilayers. Phys. Rev. B 1999, 60, 3414–3420. https://doi.org/10.1103/PhysRevB.60.3414
31. Chakka, V. M., Shan, Z. S., & Liu, J. P. Effect of coupling strength on exchange spring magnets. J. Appl. Phys. 2003, 94, 6673–6677. https://doi.org/10.1063/1.1621712
32. Hong, Y. K., Bae, S., Park, J., Choi, M., Lee, W. C., Yeo, C. D., Lee, W. Y. et al. (2025). Analytical maximum energy product model for rare-earth-free magnets. IEEE Trans. Magn. 2025, in press.
33. D. Suess, J. Lee, J. Fidler, T. Schrefl, "Exchange-coupled perpendicular media. J. Magn. Magn. Mater. 2009, 321, 545–554. https://doi.org/10.1016/j.jmmm.2008.06.041
34. Introduction to the Theory of Ferromagnetism; Oxford University Press: Oxford, UK, 1996.
35. Skomski, R.; Coey, J.M.D. Permanent Magnetism; Institute of Physics: Bristol, UK, 1999.
36. R. Skomski, J.P. Liu, D. J. Sellmyer, Quasicoherent nucleation mode in two-phase nanomagnets. Phys. Rev. B 1999, 60, 7359–7364. https://doi.org/10.1103/PhysRevB.60.7359
37. J. S. Jiang, Magnetization processes in core/shell exchange-spring structures. J. Appl. Phys. 2015, 117, 17A734; doi: 10.1063/1.4916543
38. Silva, L. F. S., Oliveira, L. L., Nunes, M. S., Dantas, A. L., & Carriço, A. S. Enhanced high-energy products of spherical hard@soft magnetic core@shell nanoparticles. J. Alloys Compd. 2025, 181684. https://doi.org/10.1016/j.jallcom.2025.181684.
39. [1] A. Vansteenkiste, J. Leliaert, M. Dvornik, M. Helsen, F. Garcia-Sanchez, and Van Waeyenberge Bartel The design and verification of MuMax3. AIP Adv. 2014, 4, 107133 doi:10.1063/1.4899186
40. Leliaert, J., Dvornik, M., Mulkers, J., De Clercq, J., Milošević, M. V., & Van Waeyenberge, B. (2018). Fast micromagnetic simulations on GPU—recent advances made with mumx3 J. Phys. D Appl. Phys. 2018, 51, 123002 https://doi.org/10.1088/1361-6463/aaab1c
41. Leliaert, J., & Mulkers, J. Tomorrow's micromagnetic simulations. J. Appl. Phys. 2019, 125, 180901. https://doi.org/10.1063/1.5093730.
42. Sun, S., Murray, C. B., Weller, D., Folks, L., & Moser, A. Monodisperse FePt nanoparticles and ferromagnetic FePt nanocrystal superlattices. Science 2000, 287, 1989–1992. https://doi.org/10.1126/science.287.5460.1989
43. Abel, F. M., Tzitzios, V., Devlin, E., Alhassan, S., Sellmyer, D. J., & Hadjipanayis, G. C. Enhancing the ordering and coercivity of L10 FePt nanostructures with bismuth additives for applications ranging from permanent magnets to catalysts. ACS Appl. Nano Mater. 2019, 2, 3146–3153. http://dx.doi.org/10.1021/acsanm.9b00463.
44. Tzitzios, V., Niarchos, D., Hadjipanayis, G., Devlin, E. and Petridis, D., Synthesis and Characterization of L10 FePt Nanoparticles from Pt(Au, Ag)/γ-Fe2O3 Core–Shell, Nanoparticles. Adv. Mater., 2005, 17, 2188-2192. https://doi.org/10.1002/adma.200500365
45. Zafiropoulou, I., Devlin, E., Boukos, N., Niarchos, D., Petridis, D., Tzitzios, V., Direct Chemical Synthesis of L10 FePt Nanostructures, Chemistry of Materials, 2007, 19, 1898-1900, https://doi.org/10.1021/cm070323v
46. Tzitzios, V., Basina, G., Tzitzios, N., Alexandrakis, V., Hu, X., & Hadjipanayis, G., Direct liquid phase synthesis of ordered L1 0 FePt colloidal particles with high coercivity using an Au nanoparticle seeding approach. New Journal of Chemistry,2016, 40(12), 10294-10299.
47. Liu, X., Sooryakumar, R., Gutierrez, C. J., & Prinz, G. A. Exchange stiffness and magnetic anisotropies in bcc $Fe_{1-x}Co_x$ alloys. J. Appl. Phys. 1994, 75, 7021–7023. https://doi.org/10.1063/1.356763

 doi:10.20944/preprints202603.1748.v1

48. Vock, S., Hengst, C., Wolf, M., Tschulik, K., Uhlemann, M., Sasvári, Z., Neu, Vet al. Magnetic vortex observation in FeCo nanowires by quantitative magnetic force microscopy. J. Magn. Magn. Mater. 2017, 443, 378–384. https://doi.org/10.1063/1.4900998
49. Rotarescu, C., Moreno, R., Fernández-Roldan, J. A., Trabada, D. G., Nemes, N. M., Fehér, T., Chubykalo-Fesenko, O. et al. Effective anisotropies in magnetic nanowires using the torque method J. Magn. Magn. Mater. 2017, 443, 378–384. https://doi.org/10.1016/j.jmmm.2017.07.059
50. Tzitzios, V., Basina, G., Niarchos, D., Li, W., & Hadjipanayis, G., Synthesis of air stable FeCo nanoparticles. Journal of Applied Physics,2011, 109, 07A313. https://doi.org/10.1063/1.3540387
51. Burkert, T., Nordström, L., Eriksson, O., & Heinonen, O. Giant magnetic anisotropy in tetragonal FeCo alloys. Phys. Rev. Lett. 2004, 93, 027203. https://doi.org/10.1103/PhysRevLett.93.027203
52. Hasegawa, T., Kanatani, S., Kazaana, M., Takahashi, K., Kumagai, K., Hirao, M., & Ishio, S. Conversion of FeCo from soft to hard magnetic material by lattice engineering and nanopatterning. Sci. Rep. 2017, 7, 13215. DOI:10.1038/s41598-017-13602-x
53. Warnicke, P., Andersson, G., Björck, M., Ferré, J., & Nordblad, P. Magnetic anisotropy of tetragonal FeCo/Pt (001) superlattices. Phys. Condens. Matter 2007, 19, 226218. 10.1088/0953-8984/19/22/226218.
54. Giannopoulos, G., Salikhov, R., Zingsem, B., Markou, A., Panagiotopoulos, I., Psycharis, V., Farle M, Niarchos, D. Large magnetic anisotropy in strained Fe/Co multilayers on AuCu and the effect of carbon doping. APL Mater. 2015, 3, 041101. https://doi.org/10.1063/1.4919058
55. Gong, M., Kirkeminde, A., Wuttig, M., & Ren, S. Phase transformation-induced tetragonal FeCo nanostructures. Nano Lett. 2014, 14, 6493–6498. https://doi.org/10.1021/nl5030485
56. Crisan, O., Crisan, A. D., Schinteie, G., & Kuncser, V. Highly Coercive $L1_0$-Phase Dots Obtained through Low Temperature Annealing for Nano-Logic Magnetic Structures. Coatings 2023, 13, 2068. https://doi.org/10.3390/coatings13122068
57. Weller, D., Moser, A., Folks, L., Best, M. E., Lee, W., Toney, M. F., Thiele J-U, Doerner, M. F. et al. High Ku materials approach to 100 Gbits/in^2. IEEE Trans. Magn. 2000, 36, 10–15. https://doi.org/10.1109/20.824418
58. Belashchenko, K. D. Anisotropy of exchange stiffness and its effect on the properties of magnets. J. Magn. Magn. Mater. 2004, 270, 413–424. https://doi.org/10.1016/j.jmmm.2003.09.017
59. Guerra, Y., Viana, B. C., & Padrón-Hernández, E. FMR by micromagnetic simulation in modulated FeCo nanowires. J. Supercond. Nov. Magn. 2022, 35, 825–831. https://doi.org/10.1007/s10948-021-06114-3.
60. Viñas, S. L., Salikhov, R., Bran, C., Palmero, E. M., Vazquez, M., Arvan, B., Farle, M et al. Magnetic hardening of $Fe_{30}Co_{70}$ nanowires. Nanotechnology 2015, 26, 415704. https://doi.org/10.1088/0957-4484/26/41/415704
61. Ullah, A., Balasubramanian, B., Tiwari, B., Giri, B., Sellmyer, D. J., Skomski, R., & Xu, X. Topological spin textures and topological Hall effect in centrosymmetric magnetic nanoparticles. Phys. Rev. B 2023, 108, 184432. https://doi.org/10.1103/PhysRevB.108.184432.
62. Breth, L., Süss, D., Vogler, C., Bergmair, B., Fuger, M., Heer, R., & Brueckl, H. Thermal switching field distribution of a single domain particle for field-dependent attempt frequency. Appl. Phys. 2012, 112, 023903. https://doi.org/10.1063/1.4737413
63. Suess, D., Schrefl, T., Fähler, S., Kirschner, M., Hrkac, G., Dorfbauer, F., & Fidler, J. Exchange spring media for perpendicular recording. Appl. Phys. Lett. 2005, 87, 012504. https://doi.org/10.1063/1.1951053
64. Trench, A., & Sykes, J. P. Rare earth permanent magnets and their place in the future economy. Engineering 2020, 6, 115–118. https://doi.org/10.1016/j.eng.2019.12.007